DEAL: Decoupled Classifier with Adaptive Linear Modulation for Group Robust Early Diagnosis of MCI to AD Conversion

Donggyu Lee, Juhyeon Park, and Taesup Moon, *Member, IEEE*

***Abstract*— While deep learning-based Alzheimer's disease (AD) diagnosis has recently made significant advancements, particularly in predicting the conversion of mild cognitive impairment (MCI) to AD based on MRI images, there remains a critical gap in research regarding the group robustness of the diagnosis. Although numerous studies pointed out that deep learning-based classifiers may exhibit poor performance in certain groups by relying on unimportant attributes, this issue has been largely overlooked in the early diagnosis of MCI to AD conversion. In this paper, we present the first comprehensive investigation of the group robustness in the early diagnosis of MCI to AD conversion using MRI images, focusing on disparities in accuracy between groups, specifically sMCI and pMCI individuals divided by age. Our experiments reveal that standard classifiers consistently underperform for certain groups across different architectures, highlighting the need for more tailored approaches. To address this, we propose a novel method, dubbed DEAL (DEcoupled classifier with Adaptive Linear modulation), comprising two key components: (1) a linear modulation of features from the penultimate layer, incorporating easily obtainable age and cognitive indicative tabular features, and (2) a decoupled classifier that provides more tailored decision boundaries for each group, further improving performance. Through extensive experiments and evaluations across different architectures, we demonstrate the efficacy of DEAL in improving the group robustness of the MCI to AD conversion prediction.**

***Index Terms*— Alzheimer's disease diagnosis, MRI, group robust classification, multimodal network.**

 This paper is supported in part by the National Research Foundation of Korea (NRF) grant [No.2021R1A2C2007884, RS-2023-00265406], Institute of Information & communications Technology Planning & Evaluation (IITP) grants [RS-2021-II211343, RS-2021-II212068, RS-2022-II220113, RS-2022-II220959] funded by the Korean government (MSIT), AOARD Grant No. FA2386-23-1-4079, SNU-Naver Hyperscale AI Center, and Hyundai Motor Chung Mong-Koo Foundation. *(Donggyu Lee and Juhyeon Park are co-first authors.) (Corresponding author: Taesup Moon.)*

Donggyu Lee is with the Department of Electrical and Computer Engineering, Sungkyunkwan University, Suwon 16419, South Korea. (e-mail: ldk308@skku.edu).

Juhyeon Park is with the Interdisciplinary Program in Artificial Intelligence, Seoul National University, Seoul 08826, South Korea. (e-mail: parkjh9229@snu.ac.kr).

Taesup Moon is with the Department of Electrical and Computer Engineering, Automation and Systems Research Institute, Institute of New Media and Communications, Interdisciplinary Program in Artificial Intelligence, and Artificial Intelligent Institute, Seoul National University, Seoul 08826, South Korea. (e-mail: tsmoon@snu.ac.kr).

I. Introduction

Alzheimer's disease (AD) is a progressive neurodegenerative disorder that significantly impacts both individuals and society. Recent trends indicate a growing prevalence of AD, with millions of individuals affected worldwide [1]. The risk of developing AD increases with age [2], [3], and nearly two-thirds of Americans with AD are 75 or older [1]. This age-related trend underscores the critical need for early diagnosis and intervention, as an aging population will lead to a greater societal and healthcare burden. The importance of early diagnosis is particularly evident at the mild cognitive impairment (MCI) stage, which represents a transitional phase between normal aging and more serious conditions like AD [4], [5]. MCI can be categorized into two types: stable MCI (sMCI), where the condition remains relatively constant over time, and progressive MCI (pMCI), where the condition is likely to worsen and develop into AD within a certain period, typically 3 years [6], [7]. Identifying whether an individual has sMCI or pMCI allows for more targeted and timely medical interventions, which can potentially slow disease progression, optimize treatment plans, and improve the quality of life for patients and their families [1], [8], [9].

In recent years, deep learning has become a cornerstone technology in the medical domain, including AD diagnosis [10], [11]. These advancements have led to significant improvements in the diagnosis and prediction of various medical conditions. However, ensuring group robustness, which guarantees that predictive models perform well across different demographic groups, should not be overlooked. Focusing solely on overall accuracy neglects potential accuracy disparities between groups, resulting in certain groups receiving inadequate care and an inefficient allocation of medical resources, along with an increased financial burden. Therefore, developing models that are robust across diverse patient demographics is crucial for delivering equitable and effective healthcare.

Despite progress in applying deep learning to medical diagnosis, a notable gap remains in research on group robustness in identifying MCI to AD conversion; specifically, in the prediction of sMCI and pMCI based on sMRI images [7], [12], [13]. While some studies have explored group robustness in other medical domains [14]–[17], the specific challenge of identifying MCI to AD conversion remains under-explored. One potential issue for addressing such a challenge arises from the age-related changes in brain structure where natural

aging processes, such as atrophy and other structural alterations, cause overlapping brain features in older adults [18]. These changes may cause the brain features of older sMCI individuals to resemble those of younger pMCI individuals [19], impeding the model's ability to accurately distinguish between these groups if the model heavily depends on the extent of brain atrophy.

Through a preliminary analysis using a ResNet-18 [20] model trained by empirical risk minimization (ERM), which is described more in detail in Section III-C. These findings suggest that certain architectures may rely heavily on brain volume reductions as a shortcut for prediction [21], rather than learning conversion-related brain features. This reliance limits their ability to distinguish between aging-related and disease-related brain changes, making models overly sensitive to sMRI similarities between groups and reducing their capacity to capture underlying causes.

To address the above issue, we propose a novel method, dubbed as **DEAL** (**DE**coupled classifier with **A**daptive **L**inear modulation). Our approach first aims to enhance feature separation between groups by linearly modulating the penultimate layer features, utilizing clinical and demographic tabular data. To ensure practicality and cost efficiency, we consider three simple tabular features: an age indicator (whether the subject is aged 75+), the mini-mental state examination (MMSE) score [22], and education level. These features are not only easily accessible but also non-invasive and require minimal resources, as they involve only a brief cognitive test and a survey. This makes them suitable for widespread clinical use without imposing significant burdens on patients and healthcare providers. We then apply a decoupled classifier with separate classification heads for groups divided by age (sMCI/pMCI under 75 and 75+) to better capture the unique characteristics of sMRI scans across these populations.

As a result of extensive experiments, we confirmed the presence of group robustness issues in baseline models and demonstrated that DEAL improves both group-balanced accuracy (GBA) and the worst-group accuracy (WGA). We showed that while simple fusion of tabular features via concatenating them with sMRI features fails to capture the complementary information between the two modalities, DEAL effectively leverages them and improves performance. Our ablation studies further validated the effectiveness of the linear modulation of DEAL using the three selected tabular features. Additionally, we identified that the linear modulation of DEAL markedly differentiates features among different groups, via UMAP visualization and computing Hausdorff distances [23] among the groups. Finally, experiments across varied architectures revealed that the group robustness challenge can persist across diverse architectures under ERM, while DEAL consistently improves the performance regardless of the model architectures.

The contributions of our work are summarized as follows:

- We identify overlooked group robustness issues in predicting MCI to AD conversion, specifically when considering the age to define groups for sMCI and pMCI.
- We propose a novel method that adaptively modulates sMRI features based on clinical and demographic context and employs a decoupled classifier to address accuracy disparities between the groups.
- We verify that the selected cost-effective tabular features effectively enhance the group robustness of classification, and that the group robustness problems persist across different architectures. Furthermore, we demonstrate that DEAL is model-agnostic and consistently improves GBA and WGA.

II. Related Works

A. Group Robustness of a Classifier

Deep neural network (DNN)-based image classifiers may perform poorly on certain subsets of data, or groups, by heavily relying on certain features that may not be relevant to the target labels [21]. For example, a DNN-based image classifier trained on ImageNet [24] is known to be biased towards recognizing textures rather than shapes [25]. The spurious feature is not always an explicit, human-recognizable feature; rather, there is a case where the model uses the implicit feature as a cue for classification, which is difficult for humans to perceive [21].

To address this issue, the group robustness classification framework was introduced, aiming to improve the accuracy of the worst-performing groups. In this framework, a group $\mathcal{G}$ is typically defined as the Cartesian product of a label set $\mathcal{Y}$ and an attribute $\mathcal{A}$ that could influence the model's behavior [26], i.e., $\mathcal{G} = \mathcal{Y} \times \mathcal{A}$

When group annotations are fully available and the spurious attribute is explicit, GroupDRO [26] is a leading algorithm that minimizes the worst-case loss through group-weighted stochastic gradient descent, explicitly focusing on the worst-performing group. Another effective approach, SUBG [27], involves sub-sampling the larger groups to create a balanced training dataset across groups. By reducing the size of overrepresented groups, the model is encouraged to pay more attention to the underrepresented groups, which can improve the performance of the worst-performing groups without increasing training costs. In cases where group annotations are available for held-out data, DFR [28] demonstrated that retraining the last layer using a group-balanced held-out data can provide performance competitive with state-of-the-art approaches. Although numerous works have been introduced to reduce the burden of acquiring group annotations, we mainly consider GroupDRO, SUBG, and DFR as our baselines, since the data in our problem setting are fully group-annotated.

B. Early Diagnosis of MCI to AD conversion

Early diagnosis of MCI to AD conversion, classifying sMCI and pMCI, is crucial for timely intervention and improved patient outcomes. Deep learning models, particularly those using MRI scans, have been developed to predict MCI to AD conversion by identifying early indicators of disease progression through neuroimaging.

Several works have proposed 2D vision transformer-based (ViT) architectures which process 2D MRI slices as input [29], [30]. One approach uses mid-sagittal images sampled from 3D MRI scans and processes them through a ViT-based model [29]. Another study introduced an architecture combining a

Swin transformer [31] and a convolutional neural network (CNN)-based module, incorporating features based on the discrepancy between each patient's age and its predicted value [30]. In addition, a transfer learning-based multi-stream CNN has been proposed to identify subtle brain differences between sMCI and pMCI, which employs AD/CN classification for pre-training and effectively captures relevant patch-based features from key anatomical landmarks [32].

Meanwhile, some methods have been developed to process 3D MRI images directly, avoiding the need for extensive preprocessing steps such as ROI-based voxel extraction. One method introduced a 3D CNN architecture pre-trained on AD and cognitively normal (CN) subjects classification [33]. A different approach utilized two 3D CNN architectures: one to predict the patient age and the other for predicting MCI to AD conversion [34]. Then, the age prediction network, trained on CN MRI images, adjusts the output of the conversion prediction network. Yet another method applied class activation maps from three models trained on classification tasks of AD/CN, low/high ADAS-11 score, and low/high CDR-SB score to guide intermediate feature maps during training for sMCI/pMCI classification [35]. Furthermore, an ordinal estimation framework has been proposed to reflect the progressive nature of AD, from CN to MCI to AD [13].

In addition to approaches that rely solely on MRI images, there have been attempts to incorporate demographic or diagnosis-related features to enhance the model's predictions [12], [36]–[39]. Wolf *et al.* [12] employed nine tabular features including demographic variables as well as task-relevant features, e.g., biomarkers of Aβ_{42}, P-tau181, T-tau, etc. This approach modifies the feature map before the global average pooling layer based on these tabular features. On the other hand, Lee *et al.* [39] attempted to integrate the information of single nucleotide polymorphisms (SNPs) and that of 3D MRI scan. In addition, several works devised architectures to fuse information from 3D MRI and positron emission tomography (PET) images [36]–[38].

Most previous studies have focused on improving diagnosis performance, typically evaluated with accuracy or AUROC. Our work has a distinct contribution in that we consider the group robustness in the early diagnosis of MCI to AD conversion, which has been a neglected problem so far. Furthermore, we utilize easily obtainable tabular features rather than invasive biomarkers like $A\beta_{42}$ employed in [12], making our method more practical for real-world applications.

C. Group Robust Classification in Medical Imaging

There have been attempts to develop group robust classifiers in the field of medical imaging. Some works have focused on mitigating biased predictions in the classification of pneumonia using chest X-rays (CXR) [14], [15]. In addition, group robustness issues in the classification of pneumothorax using CXRs and ischemic heart disease based on abdominopelvic computed tomography images have been explored [15]. Age-related performance differences have also been examined in HIV diagnosis using MRI scans [16]. In skin lesion classification, an automated skin tone detection method was developed to label skin tones and apply debiasing techniques, which helped reduce performance disparities between lighter and darker skin tones [17].

TABLE I
DEMOGRAPHICS OF DATASET

Diagnosis	CN	MCI		AD
		sMCI	pMCI	
# subjects (M / F)	883 (382 / 501)	453 (274 / 179)	228 (132 / 96)	408 (230 / 178)
Age	72.35 ± 6.62	72.14 ± 7.56	74.02 ± 7.15	74.90 ± 7.83
Education	16.52 ± 2.50	16.19 ± 2.71	16.01 ± 2.79	15.26 ± 2.91
MMSE	29.08 ± 1.10	28.11 ± 1.61	26.75 ± 1.72	23.16 ± 2.22

Values are shown as mean ± standard deviation (SD).
M = Male, F = Female

III. PROBLEM SETTING

A. Data Collection

Data used in the preparation of this article were obtained from the Alzheimer's Disease Neuroimaging Initiative (ADNI) database (adni.loni.usc.edu) [40]. The ADNI was launched in 2003 as a public-private partnership, led by Principal Investigator Michael W. Weiner, MD. The primary goal of ADNI has been to test whether serial MRI, PET, other biological markers, and clinical and neuropsychological assessment can be combined to measure the progression of MCI and early Alzheimer's disease.

We used baseline T1-weighted MRI images from the ADNI-1/GO/2/3 study cohorts, acquired during the initial screening of subjects from the database. The images are derived from 1.5T (ADNI-1) and 3T (ADNI-GO/2/3) MRI devices. The subjects are divided into three diagnostic categories: CN, MCI, AD. For MCI subjects, we further labeled them as either pMCI, who progressed to AD within 36 months from the baseline, or sMCI, who did not develop AD in the 36 months following the baseline. To reduce potential label ambiguities, we excluded subjects who reverted to MCI or CN status among those labelled as pMCI. The demographic characteristics of the dataset are shown in Table I.

B. Data Preprocessing

We downloaded the images in the DICOM format from the ADNI database and converted them to the NIfTI format. Then, the images were preprocessed using ANTsPyNet [41] under the following steps: brain extraction, N4 bias field correction [42], and SyN non-linear registration [43] into MNI standard space using T1-weighted MNI152 template with 1mm resolution. The processed images have an identical size of $192 \times 218 \times 192$.

C. Analyses on Group Robustness

In this section, we focus on examining potential accuracy disparities across different groups in the prediction of MCI to AD conversion. While the conversion prediction models typically emphasize overall accuracy, such an approach may

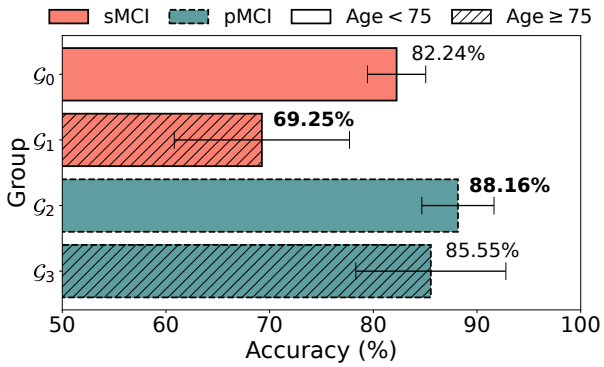

Fig. 1. Groupwise accuracy on the test sets of the MCI to AD conversion prediction task. The results are averaged over 16 different runs. The error bars represent the standard deviation.

hide significant variations in groupwise performance. Understanding these disparities is crucial, as they can significantly impact the fairness of diagnostic outcomes and healthcare interventions.

To that end, we divided the MCI cohort into four groups based on age and diagnosis: $\mathcal{G}_0$ (sMCI individuals under 75), $\mathcal{G}_1$ (sMCI individuals aged 75 or older), $\mathcal{G}_2$ (pMCI individuals under 75), and $\mathcal{G}_3$ (pMCI individuals aged 75 or older). We categorize the groups based on age to examine whether the model relies heavily on the extent of brain atrophy and can differentiate between changes due to natural aging and those associated with disease progression.

For this analysis, we trained a 3D ResNet-18 model [20], pre-trained on an AD/CN classification task, following standard transfer learning approaches in MCI to AD conversion prediction tasks [6], [7], [44]. More training details are described in Section V-C. To ensure the robustness of our analysis, we conducted 16 independent runs and report the groupwise accuracy on the test sets, with the best-performing model achieving the highest accuracy on the validation sets.

Our analysis revealed significant disparities in groupwise accuracy. Notably, accuracy for $\mathcal{G}_1$ was 69.25%, compared to 88.16% for $\mathcal{G}_2$ (Figure 1). This discrepancy highlights that existing models may struggle to capture the unique characteristics of older sMCI patients, potentially leading to biased predictions that could influence clinical decision-making if not carefully considered. For example, with lower precision in identifying pMCI among older patients ($\mathcal{G}_1$ and $\mathcal{G}_3$), many older sMCI patients may be misclassified as pMCI. This can result in unnecessary follow-up tests, closer monitoring, or preventive treatments intended for those at higher risk of progressing to AD. These unnecessary interventions not only increase healthcare costs but may also place an additional burden on patients. These findings emphasize the need for robust models ensuring fair and accurate predictions across diverse patient groups and improving the overall equity and effectiveness of AD management.

IV. Method

In this section, we propose a novel approach to enhance the group robustness of DNNs in predicting MCI to AD conversion, particularly for the age-divided sMCI and pMCI groups. Our method involves fine-tuning a DNN model pre-trained on the sMRI images for AD/CN classification task while applying adaptive linear modulation to the penultimate layer features using demographic and clinical information. To further refine the classification performance, we employ a decoupled classifier that separately handles subjects across different age ranges. Our method is dubbed as DEAL (**DE**coupled classifier with **A**daptive **L**inear modulation), and the overview of the scheme is illustrated in Figure 2. The following subsections describe the key components of DEAL in details.

TABLE II
Comparison of MMSE for sMCI/pMCI Across Different Age Ranges and p-Values of t-Tests.

Age Range	sMCI		pMCI		p-value ($\times 10^{-10}$)
	# subjects	MMSE	# subjects	MMSE	
55-75 (exclusive)	288	28.27	122	26.99	0.34
75-90 (inclusive)	165	27.84	106	26.46	2.74

A. Adaptive Linear Modulation with Age and Cognitive Indicators

We build on a DNN model pre-trained to distinguish between AD and CN subjects, enriching the features relevant to AD progression, similar to the approach in [6], [7]. Formally, let $h_{\boldsymbol{\theta}}(\cdot)$ be an L-layer neural network parameterized by $\boldsymbol{\theta} = (\boldsymbol{\theta}_1, ..., \boldsymbol{\theta}_L)$, where $\boldsymbol{\theta}_l$ represents the parameters for layer l and $\boldsymbol{\theta}_L$ denotes the parameters of the last classification layer. For pre-training, we use a dataset $\mathcal{D}^{pre} = \{(\mathbf{x}_i^{pre}, y_i^{pre})\}_{i=1}^{N^{pre}}$ consisting of an sMRI image $\mathbf{x}_i^{pre}$ of subject i and the corresponding label y_i^{pre} indicating whether the diagnosis is AD or CN. The model is trained with the following objective

$$\underset{\boldsymbol{\theta}}{\text{minimize}} \frac{1}{N^{pre}} \sum_{(\mathbf{x}_i^{pre}, y_i^{pre}) \in \mathcal{D}^{pre}} \mathcal{L}_{CE}\left(h_{\boldsymbol{\theta}}(\mathbf{x}_i^{pre}), y_i^{pre}\right) \quad (1)$$

in which $\mathcal{L}_{CE}$ is the cross-entropy loss function.

For the MCI to AD conversion prediction task, our goal is to enhance the group robustness of the sMRI-based DNN model by making features from each group more distinguishable. To achieve this, we fine-tune the pre-trained model by linearly modulating the penultimate layer features using complementary demographic and clinical information, inspired by the FiLM approach [45]. We consider an MCI dataset $\mathcal{D} = \{(\mathbf{x}_i, y_i, \mathbf{t}_i)\}_{i=1}^{N}$ that includes additional tabular information $\mathbf{t}_i \in \mathbb{R}^T$, where T represents the number of features for each subject i. This tabular data may include demographic variables like age or gender, as well as clinical features such as cerebrospinal fluid (CSF) biomarkers, ApoE4 status, and cognitive assessments.

Formally, given the penultimate layer feature vector $\mathbf{f}_i := h_{\boldsymbol{\theta}_{1:L-1}}(\mathbf{x}_i) \in \mathbb{R}^D$ for subject i, we modulate this feature with a scale factor $\boldsymbol{\gamma}_i := \gamma_\phi(\mathbf{t}_i)$ and a shift factor $\boldsymbol{\beta}_i := \beta_\psi(\mathbf{t}_i)$, which are the outputs of learnable functions $\gamma_\phi(\cdot)$ and $\beta_\psi(\cdot)$ applied to the tabular data $\mathbf{t}_i$. In our implementation, the functions $\gamma_\phi(\cdot)$ and $\beta_\psi(\cdot)$ are multi-layer perceptron (MLP)-based neural networks parameterized by ϕ and ψ, respectively.

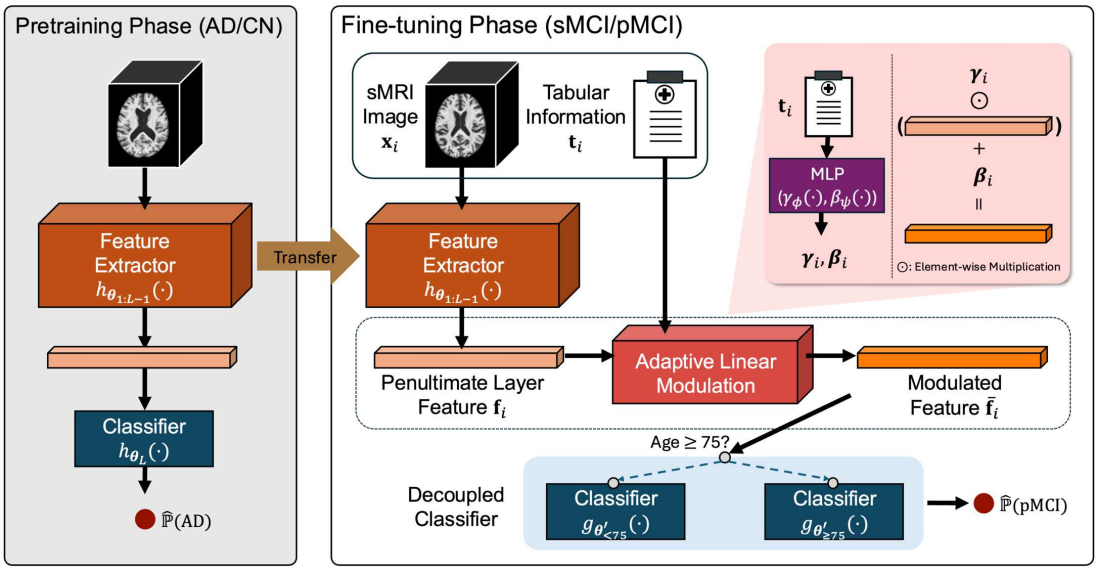

Fig. 2. Overview of our proposed approach, DEAL, which uses a decoupled classifier with adaptive linear modulation for group robust early diagnosis of MCI to AD conversion. The adaptive linear modulation leverages the age indicator, MMSE, and education level of a subject i. Based on the subject's age, the model selects one of two different classifiers.

Then, the modulated feature $\bar{\mathbf{f}}_i$ is computed as:

$$\bar{\mathbf{f}}_i = \boldsymbol{\gamma}_i \odot \mathbf{f}_i + \boldsymbol{\beta}_i \tag{2}$$

where $\odot$ denotes element-wise multiplication. This allows the model to adaptively adjust the features based on the demographic and clinical context provided by $\mathbf{t}_i$. This adaptive modulation can help improve the separation between groups in the feature space, enhancing the model's ability to distinguish between them. To ensure this approach is practical and accessible for clinical application, we select three non-invasive, easily obtainable features for the linear modulation: an age indicator (indicating whether a subject is aged 75+), MMSE score [22], and education level.

The age indicator is used to help account for natural cognitive decline with aging, since brain atrophy and reduced cognitive function can resemble early neurodegenerative patterns. This overlap can cause confusion between older sMCI and younger pMCI subjects, whose brain features may appear similar. Previous studies confirm that age-related brain changes can mimic neurodegenerative signs in pMCI, complicating their distinction through imaging biomarkers [18], [19]. By incorporating the age indicator, we aim to improve the model's ability to differentiate between these groups.

In addition to the age indicator, we utilize MMSE scores and education levels to further refine feature separability. The MMSE is a universally adopted cognitive screening tool due to its simplicity, requiring only 5-10 minutes to administer without needing specialized personnel [22], [46], [47]. Since pMCI subjects, defined as those who progress to AD within a short period (three years in our study), tend to have more severe cognitive impairment than sMCI subjects, MMSE scores can provide valuable supplementary information when brain imaging alone is not enough. Our analysis shows that MMSE scores differ significantly between sMCI and pMCI subjects across different age ranges (55-75 and 75-90), with statistically significant p-values from t-tests in Table II. Moreover, as MMSE scores can be influenced by an individual's education level [48], [49], we include it to account for this variability. These features are easier to acquire than invasive biomarkers like CSF, which reduces burden on patients and medical facilities, and ensures effective and practical modulation of sMRI-based features.

B. Age-based Decoupled Classifier

Decoupling a classifier can be beneficial when the optimal classifiers for two data distributions divided by an attribute have a large disagreement [50]. We assume that disagreement between the optimal classifiers of $(\mathcal{G}_0, \mathcal{G}_2)$ and $(\mathcal{G}_1, \mathcal{G}_3)$ exists considering that difference in the brain characteristics and pathology between younger and older subjects [51]. Moreover, we expect that the decoupled classifier is better at capturing distinct patterns of cognitive decline and sMRI features across two age ranges (under 75 and 75 or older) while a single classifier may not adequately account for these variations.

Specifically, our model shares a common feature extraction body, $h_{\boldsymbol{\theta}_{1:L-1}}(\mathbf{x}_i)$, which processes the input sMRI scan $\mathbf{x}_i$ into a modulated feature vector $\bar{\mathbf{f}}_i$. After the feature extraction and modulation, the model utilizes a decoupled classifier $g_{\boldsymbol{\theta}'_{\text{age}(i)}}(\cdot)$, which applies one of two classification heads depending on the subject's age: one with parameters $\boldsymbol{\theta}'_{<75}$ for subjects under 75 and another with parameters $\boldsymbol{\theta}'_{\geq 75}$ for those aged 75 and older. These classification heads are designed to map the feature vector $\bar{\mathbf{f}}_i$ to the target labels (sMCI or pMCI) in an age-specific manner. The overall objective is to minimize the average cross-entropy loss over *all* parameters:

$$\underset{\substack{\boldsymbol{\theta}_{1:L-1},\,\phi,\,\psi \\ \boldsymbol{\theta}'_{<75},\,\boldsymbol{\theta}'_{\geq 75}}}{\text{minimize}} \frac{1}{N} \sum_{(\mathbf{x}_i, y_i, \mathbf{t}_i) \in \mathcal{D}} \mathcal{L}_{CE}(g_{\boldsymbol{\theta}'_{\text{age}(i)}}(\bar{\mathbf{f}}_i), y_i) \tag{3}$$

where $\boldsymbol{\theta}'_{\text{age}(i)}$ is determined by the subject's age:

$$\boldsymbol{\theta}'_{\text{age}(i)} = \begin{cases} \boldsymbol{\theta}'_{\geq 75} & \text{if the age of subject } i \geq 75, \\ \boldsymbol{\theta}'_{<75} & \text{otherwise.} \end{cases} \quad (4)$$

V. Experiments

A. Baseline Methods

We evaluate our method by comparing it to several baselines, categorized into four types. Type I includes unimodal approaches that use either sMRI images or tabular information as input data. Empirical Risk Minimization (ERM) serves as the baseline trained with standard cross-entropy loss on sMRI data, while ERM-T is a logistic regression model that only utilizes the same tabular information features as our method: age indicator, MMSE scores, and education level. This serves as a benchmark for tabular-only classifiers. In addition, we adopt Hope [13], a structured approach that classifies pMCI and sMCI using prototypes derived from AD and CN subjects by leveraging the ordinal nature of disease progression.

Type II consists of methods that combine sMRI data with the same tabular information used in our approach. The Concat-1FC and Concat-2FC methods [12] are simple approaches that concatenate these tabular features with the sMRI-based features at the penultimate layer, allowing the classifier to use this combined representation. FiLM [45] and DAFT [12] are more advanced methods, applying affine transformations within the ResNet architecture, similar to our method. These methods adaptively transform features to better incorporate multi-modal information. Additionally, We also compare DAFT using its original tabular features to assess the impact of different feature settings on model performance.

Type III includes widely used baselines for comparing performance in group robustness problems, such as GroupDRO [26], DFR [28], and SUBG [27]. While these methods are not specific to sMRI data, they are commonly applied to various models to ensure consistent performance across groups. We include them to evaluate their effectiveness in handling group robustness when applied to both sMRI-only models and models integrating sMRI and tabular data. For the latter, we extend them with a naive Concat-based approach, concatenating tabular features with sMRI features at the penultimate layer. This setup allows us to assess whether these methods can enhance performance, particularly in maintaining consistency across groups like older sMCI patients.

Type IV involves our proposed method and its variations. We evaluate the performance of using the same tabular features as in the main method and also test an additional feature, gender, to explore its effect on classification.

B. Evaluation Metrics

To assess the performance of our binary classification task, we use several standard evaluation metrics, including accuracy, AUROC, F1-score, sensitivity, and specificity. These metrics provide a comprehensive view of the model's ability to correctly classify pMCI and sMCI subjects.

In addition to these metrics, we measure the group robustness of each method using group-balanced accuracy (GBA), which averages accuracy across all groups to give each group equal weight and the worst-group accuracy (WGA), defined as the minimum accuracy across groups to highlight the performance of the model on the most challenging group. Together, these metrics provide a comprehensive view of each method's consistency across groups, and its overall groupwise performance.

It is important to note that all results are averaged over 16 independent runs to ensure reliable evaluation, using 4 test sets and 4 validation sets per test set. As such, each reported metric is the mean value across these runs. Specifically, WGA is computed for each run and then averaged, which means it may differ from the minimum of the groupwise accuracies presented in the results table.

C. Implementation Details

We implemented 3D ResNet-18 models using MONAI [52] with Python 3.7.13, PyTorch 1.13.1 [53]. We used the AdamW optimizer [54] with a weight decay of 0.001, β_1 of 0.9, β_2 of 0.999, and ϵ of 1e-8. Learning rates were selected based on the highest GBA: [5e-6, 5e-5] for fine-tuning pre-trained models (for ViT [55] in Section V-G, [1e-6, 5e-6]), and [1e-4, 1e-3] for training from scratch. The cosine annealing strategy was applied for learning rate scheduling, with the maximum number of iterations set equal to the training epochs. Models were trained for 50 and 100 epochs when they were fine-tuned and trained from scratch respectively, using a batch size of 4 (for EfficientNet [56] in Section V-G, 8). Data augmentation included random flipping and affine transformations with a probability of 0.5 using TorchIO [57]. Images are z-normalized and clamped between [-0.5, 2.5] to handle outliers, similar to the approach in [58]. To address the class imbalance between pMCI and sMCI samples, we applied weighted cross-entropy loss, with weights proportional to the sample ratio in the training dataset. For $\gamma_\phi(\cdot)$ and $\beta_\psi(\cdot)$ of DEAL, we used a single shared linear layer that outputs both scale and shift factors (for EfficientNet, two linear layers with ReLU in between). To split the dataset, we set aside 15% of the data as the test set. The rest was split into training and validation sets, keeping a 70:15 ratio. We ensured that group proportions were consistent between the splits to avoid any imbalance. All experiments ran on AMD Ryzen Threadripper PRO 3975WX CPUs and NVIDIA RTX A5000 GPUs.

D. Main Results

We compared our method with various baseline approaches to evaluate group robustness in MCI to AD conversion prediction. Table III shows that several baseline models, including unimodal sMRI-based models like ERM and Hope (Type I), suffers from significantly lower WGA compared to GBA, underscoring group robustness challenges. In addition, the tabular-only model, ERM-T, shows weaker overall performance compared to ERM, demonstrating the limitations without sMRI data, as tabular data lacks the rich spatial details needed to capture the complexities of MCI progression.

For multimodal approaches (Type II), naively concatenating tabular features with sMRI data (Concat-1FC, -2FC) yields

TABLE III
PERFORMANCE COMPARISON OF MCI TO AD CONVERSION (SMCI/PMCI) PREDICTION TASK

Type	Method	GBA	WGA	Groupwise Accuracy				Accuracy	AUROC	F1-score	Sensitivity	Specificity
				Group $\mathcal{G}_0$	Group $\mathcal{G}_1$	Group $\mathcal{G}_2$	Group $\mathcal{G}_3$					
I	ERM	81.30 ± 3.12	68.10 ± 7.21	82.24 ± 2.90	69.25 ± 8.73	88.16 ± 3.60	85.55 ± 7.47	80.71 ± 2.42	88.34 ± 1.52	75.22 ± 2.94	86.96 ± 4.04	77.54 ± 2.95
	ERM-T	72.63 ± 5.93	62.83 ± 8.18	76.71 ± 3.76	75.00 ± 7.93	63.82 ± 9.78	75.00 ± 7.91	73.68 ± 4.89	76.75 ± 4.04	63.74 ± 6.74	68.93 ± 8.78	76.09 ± 4.61
	Hope* [13]	77.73 ± 2.11	67.04 ± 6.95	**85.37** ± 2.62	74.00 ± 9.00	75.00 ± 9.12	76.56 ± 5.35	79.39 ± 1.82	85.79 ± 2.34	71.18 ± 2.19	75.71 ± 5.11	81.25 ± 3.80
II	Concat-1FC [12]	81.85 ± 2.75	70.32 ± 7.06	82.81 ± 3.97	70.75 ± 7.55	87.50 ± 3.78	86.33 ± 5.69	81.31 ± 2.24	88.24 ± 1.64	75.82 ± 2.47	86.96 ± 3.45	78.44 ± 3.34
	Concat-2FC [12]	82.27 ± 3.06	70.74 ± 7.64	82.10 ± 2.47	71.50 ± 8.62	89.14 ± 1.31	86.33 ± 6.54	81.49 ± 2.44	88.80 ± 1.35	76.19 ± 2.74	**87.86** ± 2.85	78.26 ± 3.04
	FiLM [45]	70.38 ± 3.98	61.13 ± 4.38	76.70 ± 3.26	70.00 ± 6.53	62.17 ± 5.51	72.66 ± 9.91	71.81 ± 3.32	73.52 ± 3.72	61.46 ± 4.75	66.96 ± 7.15	74.28 ± 3.90
	DAFT [12]	71.51 ± 4.37	56.01 ± 5.74	76.42 ± 4.61	69.00 ± 11.27	62.50 ± 11.67	78.13 ± 6.03	72.36 ± 4.26	81.32 ± 4.62	62.93 ± 5.27	69.64 ± 6.83	73.73 ± 5.64
	DAFT† [12]	80.84 ± 3.49	69.56 ± 6.61	80.26 ± 4.04	**82.75** ± 8.72	86.51 ± 6.36	73.83 ± 10.51	81.01 ± 2.82	89.97 ± 1.29	74.05 ± 4.11	80.71 ± 6.88	81.16 ± 4.03
III	Decouple [59]	82.14 ± 2.17	71.43 ± 5.94	80.97 ± 3.61	72.25 ± 6.77	89.80 ± 3.02	85.55 ± 5.92	81.19 ± 1.79	88.76 ± 0.99	75.89 ± 1.94	**87.86** ± 2.45	77.81 ± 2.63
	Group DRO [26]	82.70 ± 2.88	71.88 ± 6.19	82.93 ± 3.10	72.25 ± 6.60	88.49 ± 2.12	**87.11** ± 6.23	82.03 ± 2.26	88.33 ± 1.50	76.71 ± 2.71	**87.86** ± 3.21	79.08 ± 2.64
	Group DRO + Concat	82.39 ± 2.79	70.74 ± 7.21	82.95 ± 2.99	71.00 ± 7.51	88.49 ± 3.44	**87.11** ± 6.23	81.73 ± 2.16	88.47 ± 1.40	76.41 ± 2.51	**87.86** ± 3.21	78.62 ± 2.72
	DFR [28]	80.14 ± 2.98	66.19 ± 8.17	81.53 ± 3.84	66.25 ± 8.24	86.84 ± 5.58	85.93 ± 6.81	79.51 ± 2.44	87.14 ± 2.37	73.95 ± 2.72	86.43 ± 5.39	76.00 ± 4.22
	DFR + Concat	80.79 ± 3.79	69.52 ± 6.54	81.53 ± 4.60	71.00 ± 6.85	87.82 ± 7.83	82.81 ± 9.75	80.35 ± 2.98	88.10 ± 2.54	74.46 ± 4.27	85.54 ± 7.86	77.72 ± 4.28
	SUBG [27]	81.89 ± 3.31	71.99 ± 8.25	83.24 ± 2.86	72.25 ± 8.45	86.51 ± 3.31	85.55 ± 6.34	81.55 ± 2.92	88.55 ± 1.52	75.90 ± 3.28	86.07 ± 3.27	79.26 ± 3.84
	SUBG + Concat	81.69 ± 2.94	72.24 ± 7.17	82.95 ± 2.62	72.75 ± 7.75	85.53 ± 4.07	85.55 ± 5.91	81.37 ± 2.40	88.11 ± 1.64	75.58 ± 2.76	85.54 ± 3.53	79.26 ± 3.25
IV	DEAL	**84.61** ± 3.48	**78.69** ± 6.38	85.09 ± 5.57	80.75 ± 6.89	**89.80** ± 6.22	82.81 ± 5.82	**84.56** ± 3.69	**90.92** ± 0.83	**79.18** ± 4.25	86.61 ± 4.14	**83.51** ± 5.34
	DEAL+ Gender	83.21 ± 3.15	75.45 ± 6.84	83.81 ± 5.55	78.75 ± 7.26	89.80 ± 5.91	80.47 ± 7.86	83.17 ± 3.19	90.40 ± 1.49	77.46 ± 3.59	85.54 ± 4.94	81.97 ± 5.15

Values are shown as mean ± SD. Note that results are computed for each run and averaged over 16 runs. Thus, WGA may not exactly match the minimum of the averaged groupwise accuracies.
* denotes the models trained from scratch. The others are fine-tuned from the models trained on AD/CN classification task.
† denotes the models used tabular features introduced in DAFT [12] including Aβ_{42}, P-tau181, and T-tau.

minimal improvement. More advanced methods like FiLM and DAFT, which apply feature transformations within the ResNet blocks, might struggle to learn informative representation with the tabular features we used, resulting in markedly lower overall performance compared to ERM. While DAFT†, when used with its original invasive biomarkers, achieves higher overall accuracy compared to ERM and improves $\mathcal{G}_1$ accuracy, it suffers from lower accuracy of $\mathcal{G}_3$. This indicates that the group robustness challenge still persists. Furthermore, the invasive nature of the biomarkers makes DAFT less practical due to the difficulty in obtaining these features.

Group robustness-specific baselines (Type III) such as GroupDRO and SUBG show little improvement over ERM. These approaches are effective when there exists large group imbalance, or a dominating spurious feature, but may be less effective when it is mild [27]. In our case, however, the group imbalance is not extreme (see Table II for the number of subjects in each group). Furthermore, we assume that the age-based group partition may be imperfect [60] for GroupDRO to sufficiently consider the reliance on age-related brain atrophy. Additionally, due to the lack of data, up-weighting or sub-sampling may fail to generalize effectively. Moreover, even with feature concatenation, they fail to fully capture the complementary information between sMRI and tabular data, leading to not much difference in the performance.

In contrast, our proposed method, DEAL, significantly improves not only the overall performance metrics like AUROC, but also GBA and WGA with a substantial improvement in the accuracy of $\mathcal{G}_1$. This demonstrates the effectiveness of DEAL in addressing group robustness issues for the early diagnosis of MCI-AD conversion. Furthermore, when we add gender as an additional tabular feature (*i.e.,* DEAL+Gender), we observe that it does not enhance the performance, indicating that our simple feature set is effective enough for improving the group robustness of the prediction.

E. Ablation Study on the Tabular Features

To evaluate the impact of the chosen tabular features on group robustness, we conducted an ablation study using models with our adaptive linear modulation. We considered

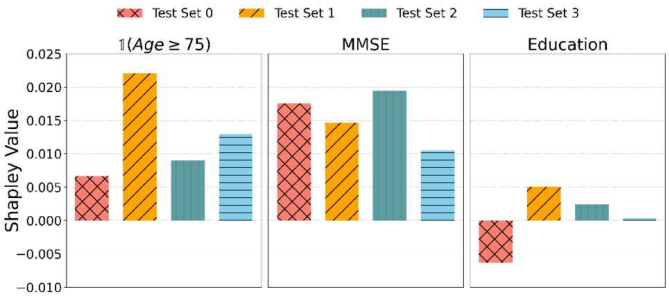

Fig. 3. Shapley values of each feature on 4 different test sets, showing the contribution of each feature to GBA.

3 features: the age indicator $\mathbb{1}(\text{Age} \geq 75)$ (D), MMSE (M), and education (E). Additionally, we included the raw age (A) feature to highlight the advantage of the age indicator over raw age. For this study, we employed models with a single classification head, to focus on the effectiveness of the linear modulation. The results are shown in Table IV.

When using individual features, the age indicator markedly enhances both GBA and WGA compared to other variables, including raw age. This suggests that the age indicator, despite being derived from age, better facilitates group-conscious transformations. Furthermore, MMSE also boosts GBA and WGA, while education alone shows no positive effect compared to the results from ERM.

For feature combinations, using both MMSE and the age indicator together results in slightly better performance than the age indicator alone, improving both GBA and WGA. The combination of MMSE and education also shows some improvement over either feature used alone. The best result is observed when all three features—age indicator, MMSE, and education—are used together. Finally, adding the decoupled classifier to this combination, DEAL, significantly boosts both GBA and WGA, demonstrating its effectiveness in enhancing the group robustness of the model.

To further analyze the contribution of each feature to GBA, we report the Shapley value [61] with four different test sets. The Shapley value of j-th feature, ϕ_j, is computed with the following formula.

TABLE IV
ABLATION STUDY ON THE COMBINATION OF TABULAR FEATURES

Tabular Feature				GBA.	WGA	Groupwise Accuracy				Accuracy	AUROC	F1-score	Sensitivity	Specificity
A	D	M	E			Group $\mathcal{G}_0$	Group $\mathcal{G}_1$	Group $\mathcal{G}_2$	Group $\mathcal{G}_3$					
✓				81.73 ± 3.50	70.17 ± 8.67	82.67 ± 3.88	70.75 ± 9.32	87.17 ± 4.69	**86.33** ± 5.69	81.19 ± 3.02	88.99 ± 1.40	75.70 ± 3.35	86.79 ± 3.88	78.35 ± 4.14
	✓			82.68 ± 2.51	74.01 ± 6.05	84.66 ± 4.35	74.25 ± 6.36	87.83 ± 4.98	83.98 ± 4.54	82.63 ± 2.96	88.95 ± 1.38	77.04 ± 3.07	86.07 ± 2.92	80.89 ± 4.76
		✓		82.53 ± 3.29	71.31 ± 7.81	87.22 ± 4.38	72.00 ± 8.76	86.51 ± 6.91	84.38 ± 6.85	82.99 ± 3.61	90.56 ± 0.95	77.34 ± 3.85	85.54 ± 4.10	81.70 ± 5.89
			✓	81.22 ± 3.43	67.57 ± 9.64	83.10 ± 3.32	68.00 ± 10.12	87.83 ± 3.71	85.94 ± 6.25	80.77 ± 2.98	88.86 ± 1.27	75.33 ± 3.18	**86.96** ± 3.61	67.57 ± 9.64
✓		✓		83.40 ± 3.30	74.06 ± 7.65	87.22 ± 4.30	74.50 ± 7.84	89.47 ± 5.08	82.42 ± 7.29	83.83 ± 3.27	90.84 ± 0.73	78.31 ± 3.70	86.25 ± 3.49	82.61 ± 4.70
	✓	✓		83.83 ± 3.37	74.36 ± 7.60	86.65 ± 5.17	76.00 ± 8.13	89.47 ± 6.92	83.20 ± 8.13	84.07 ± 3.42	90.42 ± 0.95	78.65 ± 3.82	86.61 ± 4.63	82.79 ± 5.41
	✓		✓	82.11 ± 2.20	73.60 ± 4.29	86.08 ± 2.33	74.75 ± 5.61	85.20 ± 6.15	82.42 ± 4.69	82.63 ± 2.03	88.69 ± 1.15	76.48 ± 2.62	83.93 ± 4.41	81.98 ± 2.99
		✓	✓	82.84 ± 3.08	72.29 ± 5.48	87.64 ± 3.42	72.75 ± 6.06	86.18 ± 8.13	84.77 ± 7.21	83.35 ± 2.76	90.30 ± 0.94	77.60 ± 3.42	85.54 ± 4.95	82.25 ± 4.01
✓		✓	✓	83.98 ± 2.97	75.49 ± 5.93	**87.93** ± 3.78	78.25 ± 7.15	88.49 ± 6.72	81.25 ± 7.91	**84.68** ± 2.69	**91.05** ± 0.81	78.95 ± 3.34	85.18 ± 4.57	**84.42** ± 4.01
	✓	✓	✓	84.15 ± 2.63	76.04 ± 4.40	86.79 ± 4.92	79.25 ± 5.31	88.16 ± 8.04	82.42 ± 8.60	84.56 ± 2.75	90.73 ± 0.95	78.91 ± 3.11	85.54 ± 4.36	84.06 ± 4.58
DEAL				**84.61** ± 3.48	**78.69** ± 6.38	85.09 ± 5.57	**80.75** ± 6.89	**89.80** ± 6.22	82.81 ± 5.82	84.56 ± 3.69	90.92 ± 0.83	**79.18** ± 4.25	86.61 ± 4.14	83.51 ± 5.34

Values are shown as mean ± SD. Note that results are computed for each run and averaged over 16 runs. Thus, WGA may not exactly match the minimum of the averaged groupwise accuracies.
A = Age, D = Age Indicator $\mathbb{1}(\text{Age} \geq 75)$, M = MMSE, E = Education

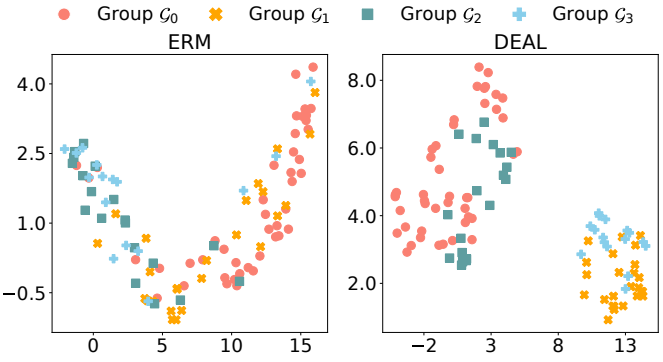

Fig. 4. UMAP plots for ERM and DEAL models. While the ERM model shows mixed features across groups, DEAL effectively separates the features by age, enabling better distinction between different groups.

TABLE V
DISTANCE BETWEEN THE RESPECTIVE GROUP FEATURES

Method	$d_H(X,Y)$		$d_A(X,Y)$	
	$\mathcal{G}_0$ vs $\mathcal{G}_2$	$\mathcal{G}_1$ vs $\mathcal{G}_3$	$\mathcal{G}_0$ vs $\mathcal{G}_2$	$\mathcal{G}_1$ vs $\mathcal{G}_3$
ERM	1.72 ± 0.92	1.48 ± 0.88	0.32 ± 0.16	0.26 ± 0.13
DEAL	2.19 ± 0.53	2.26 ± 0.69	0.66 ± 0.19	0.71 ± 0.22

Values are shown as mean ± SD.

$$\phi_j = \frac{1}{|\mathcal{F}|!} \sum_{\mathcal{S} \subseteq \mathcal{F} \setminus \{j\}} |\mathcal{S}|! \cdot (|\mathcal{F}| - |\mathcal{S}| - 1)! \cdot (\text{GBA}^{\mathcal{S} \cup \{j\}} - \text{GBA}^{\mathcal{S}}) \tag{5}$$

where $\mathcal{F}$ is a set of all features (excluding raw age (A) here) and $\text{GBA}^{\mathcal{S}}$ denotes GBA with a model trained with a set of feature $\mathcal{S}$. The positive ϕ_j indicates that j-th feature is beneficial to the improvement of GBA, and vice versa. From Figure 3, it can be checked that MMSE and the age indicator contribute to the enhancement of GBA in the majority of runs while education often contributes to this improvement.

F. Effectiveness of Linear Modulation

To validate the effectiveness of the linear modulation, we first visualized the feature space using UMAP [62], reducing the feature dimension to 2. As shown in Figure 4, the features generated by the ERM model are highly mixed, especially between $\mathcal{G}_1$ (older sMCIs) and $\mathcal{G}_2$ (younger pMCIs), likely causing the model to confuse labels due to their overlaps. In contrast, our linear modulation clearly separates the features of younger ($\mathcal{G}_0, \mathcal{G}_2$) and older subjects ($\mathcal{G}_1, \mathcal{G}_3$), thanks to the use of the age indicator.

Furthermore, within each age range, we expect the combination of tabular features to help distinguish $\mathcal{G}_0$ from $\mathcal{G}_2$, and $\mathcal{G}_1$ from $\mathcal{G}_3$, in the penultimate layer. To measure this separation, we adopt Hausdorff distance, which measures the maximum distance between two sets of points, defined as:

$$d_H(X,Y) := \max(\sup_{x \in X} d(x,Y), \sup_{y \in Y} d(y,X)) \tag{6}$$

where $d(x,Y)$ denotes the minimum distance between a point x and a set Y, defined as $d(x,Y) := \inf_{y \in Y} d(x,y)$ and d is an arbitrary distance measure. In addition, we report the average distance between the two sets defined as:

$$d_A(X,Y) := (\frac{1}{|X|} \sum_{x \in X} d(x,Y) + \frac{1}{|Y|} \sum_{y \in Y} d(y,X))/2 \tag{7}$$

We adopt ℓ_2 distance as d in our analysis. To ensure comparability of distances computed from different feature spaces, all features are standardized. Table V compares these two distance measures with features computed from the ERM model and DEAL. It can be noted that the distance of the features from DEAL between sMCI and pMCI is greater in both measures, which implies that our proposed feature transformation scheme contributes to the clearer separation between groups, leading to improved performance.

G. Architecture Variation Analysis

To ensure that the issue of the group robustness and the effectiveness of our proposed method are not limited to a specific architecture, we conducted experiments with different architectures, including 3D CNN-based architecture (3D EfficientNet [56]), 3D ViT-based architecture (3D ViT-B [55]), and 2D CNN-based architecture (2D ResNet-18 [20]). The results are presented in Table VI.

First of all, it is evident that the disparities in accuracy between groups are present across various architectures. The $\mathcal{G}_1$ exhibits a significantly lower accuracy compared to the other groups. We posit that these findings substantiate the assertion that the issue we have identified is not exclusive to

TABLE VI
RESULTS OF ARCHITECTURE VARIATION ANALYSIS

Architecture	Method	GBA	WGA	Groupwise Accuracy				Accuracy	AUROC	F1-score	Sensitivity	Specificity
				Group $\mathcal{G}_0$	Group $\mathcal{G}_1$	Group $\mathcal{G}_2$	Group $\mathcal{G}_3$					
3D EfficientNet [56]	ERM	82.19 ± 4.63	69.91 ± 8.02	**80.82** ± 2.98	70.75 ± 9.20	92.43 ± 2.69	**84.77** ± 9.94	81.13 ± 3.77	**89.47** ± 2.70	76.07 ± 4.49	**88.93** ± 5.09	77.17 ± 3.90
	DEAL	**82.64** ± 5.02	**74.62** ± 7.59	79.69 ± 3.66	**77.75** ± 9.11	**93.42** ± 4.07	79.69 ± 9.27	**81.73** ± 4.52	89.38 ± 3.22	**76.35** ± 5.33	87.14 ± 5.11	**78.99** ± 5.04
3D ViT-B [55]	ERM	77.05 ± 3.39	66.28 ± 6.21	80.11 ± 5.34	70.25 ± 9.57	78.95 ± 8.80	**78.91** ± 9.64	77.34 ± 1.95	84.21 ± 4.57	69.98 ± 3.27	78.93 ± 8.27	76.54 ± 4.46
	DEAL	**79.41** ± 4.00	**72.16** ± 6.17	**80.68** ± 2.99	**76.00** ± 8.26	**83.22** ± 8.85	77.73 ± 7.20	**79.57** ± 3.34	**88.31** ± 3.14	**72.64** ± 4.59	**80.71** ± 6.80	**78.99** ± 3.96
2D ResNet-18 [20]	ERM	71.72 ± 2.39	58.14 ± 4.93	78.69 ± 4.05	65.75 ± 9.11	63.16 ± 6.65	**79.30** ± 7.47	72.84 ± 2.59	75.71 ± 1.67	63.63 ± 2.34	**70.54** ± 4.39	74.00 ± 4.92
	DEAL	**73.73** ± 2.82	**62.30** ± 5.90	**80.68** ± 4.62	**74.75** ± 6.64	**64.47** ± 7.06	75.00 ± 8.83	**75.42** ± 2.55	**80.25** ± 1.11	**65.46** ± 3.31	69.29 ± 5.57	**78.53** ± 4.27

Values are shown as mean ± SD. Note that results are computed for each run and averaged over 16 runs. Thus, WGA may not exactly match the minimum of the averaged groupwise accuracies.

a specific architecture. Furthermore, our proposed algorithm has demonstrated efficacy in reducing the disparities in the accuracy between groups, resulting in an improvement in both GBA and WGA. We believe that these results provide compelling evidence for the generality of the issue we have raised and the effectiveness of our proposed method.

VI. CONCLUSION

In this study, we investigated the disparities in accuracy between groups, particularly sMCI and pMCI divided by age, in early diagnosis of MCI to AD conversion across different architectures. To mitigate the problem, we proposed DEAL, which has two major components; adaptive and cost-effective linear modulation of penultimate features, and a decoupled classifier. Our extensive experimental results demonstrated that the linear modulation contributes to a clearer separation of features between each group and the decoupled classifier further enhances the classification performance with more tailored decision boundaries for the different age ranges.

While our method demonstrated significant improvements, some limitations remain. The relatively small dataset may affect generalizability, and although MMSE was selected for practical reasons, other features could provide additional value across different clinical environments. Furthermore, our focus on the group robustness is currently limited to age-related factors, while this focused approach allows us to provide a detailed analysis within this context. Future work will address these issues by expanding the dataset with additional data sources and longitudinal data, incorporating practical features such as the Montreal Cognitive Assessment [63], and exploring group robustness beyond age, including more diverse populations and ethical backgrounds.

Despite these limitations, we believe our work sheds light on the overlooked issue of group robustness in the early diagnosis of MCI to AD conversion. We hope that our work stimulates further research in this area and serves as a solid baseline for future advancements.

ACKNOWLEDGMENT

Data collection and sharing for the Alzheimer's Disease Neuroimaging Initiative (ADNI) is funded by the National Institute on Aging (National Institutes of Health Grant U19 AG024904). The grantee organization is the Northern California Institute for Research and Education. In the past, ADNI has also received funding from the National Institute of Biomedical Imaging and Bioengineering, the Canadian Institutes of Health Research, and private sector contributions through the Foundation for the National Institutes of Health (FNIH) including generous contributions from the following: AbbVie, Alzheimer's Association; Alzheimer's Drug Discovery Foundation; Araclon Biotech; BioClinica, Inc.; Biogen; Bristol-Myers Squibb Company; CereSpir, Inc.; Cogstate; Eisai Inc.; Elan Pharmaceuticals, Inc.; Eli Lilly and Company; EuroImmun; F. Hoffmann-La Roche Ltd and its affiliated company Genentech, Inc.; Fujirebio; GE Healthcare; IXICO Ltd.; Janssen Alzheimer Immunotherapy Research & Development, LLC.; Johnson & Johnson Pharmaceutical Research & Development LLC.; Lumosity; Lundbeck; Merck & Co., Inc.; Meso Scale Diagnostics, LLC.; NeuroRx Research; Neurotrack Technologies; Novartis Pharmaceuticals Corporation; Pfizer Inc.; Piramal Imaging; Servier; Takeda Pharmaceutical Company; and Transition Therapeutics.

REFERENCES

[1] "2024 alzheimer's disease facts and figures," *Alzheimer's & Dementia*, vol. 20, no. 5, pp. 3708–3821, 2024.
[2] L. Hebert *et al.*, "Change in risk of alzheimer disease over time," *Neurology*, vol. 75, no. 9, pp. 786–791, 2010.
[3] J.-Q. Li *et al.*, "Risk factors for predicting progression from mild cognitive impairment to alzheimer's disease: a systematic review and meta-analysis of cohort studies," *J. Neurol. Neurosurg. Psychiatry.*, vol. 87, no. 5, pp. 476–484, 2016.
[4] R. C. Petersen, "Mild cognitive impairment as a diagnostic entity," *J. Intern. Med.*, vol. 256, no. 3, pp. 183–194, 2004.
[5] M. S. Albert *et al.*, "The diagnosis of mild cognitive impairment due to alzheimer's disease: recommendations from the national institute on aging-alzheimer's association workgroups on diagnostic guidelines for alzheimer's disease," *Focus*, vol. 11, no. 1, pp. 96–106, 2013.
[6] C. Lian, M. Liu, J. Zhang, and D. Shen, "Hierarchical fully convolutional network for joint atrophy localization and alzheimer's disease diagnosis using structural mri," *IEEE Trans. Pattern Anal. Mach. Intell.*, vol. 42, no. 4, pp. 880–893, 2020.
[7] K. Oh, Y.-C. Chung, K. W. Kim, W.-S. Kim, and I.-S. Oh, "Classification and visualization of alzheimer's disease using volumetric convolutional neural network and transfer learning," *Sci. Rep.*, vol. 9, no. 1, p. 18150, 2019.
[8] B. P. Leifer, "Early diagnosis of alzheimer's disease: Clinical and economic benefits," *J. Am. Geriatr. Soc.*, vol. 51, no. 5s2, pp. S281–S288, 2003.
[9] J. Rasmussen and H. Langerman, "Alzheimer's disease–why we need early diagnosis," *Degener. Neurol. Nueromuscul. Dis.*, vol. 9, pp. 123–130, 2019.
[10] M. Khojaste-Sarakhsi, S. S. Haghighi, S. F. Ghomi, and E. Marchiori, "Deep learning for alzheimer's disease diagnosis: A survey," *Artif. Intell. Med.*, vol. 130, p. 102332, 2022.
[11] R. Sharma, T. Goel, M. Tanveer, C. T. Lin, and R. Murugan, "Deep-learning-based diagnosis and prognosis of alzheimer's disease: A comprehensive review," *IEEE Trans. Cognit. Dev. Syst.*, vol. 15, no. 3, pp. 1123–1138, 2023.
[12] T. N. Wolf, S. Pölsterl, C. Wachinger, A. D. N. Initiative, the Australian Imaging Biomarkers, and L. flagship study of ageing, "Daft: A universal module to interweave tabular data and 3d images in cnns," *NeuroImage*, vol. 260, p. 119505, 2022.

[13] C. Wang, Y. Lei, T. Chen, J. Zhang, Y. Li, and H. Shan, "Hope: Hybrid-granularity ordinal prototype learning for progression prediction of mild cognitive impairment," *IEEE J. Biomed. Health. Inf.*, 2024.

[14] R. Marcinkevics, E. Ozkan, and J. E. Vogt, "Debiasing deep chest x-ray classifiers using intra-and post-processing methods," in *Proc. MLHC*, Durham, NC, USA, 2022, pp. 504–536.

[15] L. Luo, X. Huang, M. Wang, Z. Wan, and H. Chen, "Medical image debiasing by learning adaptive agreement from a biased council," *arXiv preprint arXiv:2401.11713*, 2024.

[16] Q. Zhao, E. Adeli, and K. M. Pohl, "Training confounder-free deep learning models for medical applications," *Nat. Commun.*, vol. 11, no. 1, p. 6010, 2020.

[17] P. J. Bevan and A. Atapour-Abarghouei, "Detecting melanoma fairly: Skin tone detection and debiasing for skin lesion classification," in *MICCAIW DART*, 2022, pp. 1–11.

[18] C. Raji, O. Lopez, L. Kuller, and O. Carmichael, "Age, alzheimer disease, and brain structure," *Neurology*, vol. 73, pp. 1899–905, 10 2009.

[19] H.-D. Nguyen, M. Clément, B. Mansencal, and P. Coupé, "Towards better interpretable and generalizable ad detection using collective artificial intelligence," *Comput. Med. Imaging Graph.*, vol. 104, p. 102171, 2023.

[20] K. He, X. Zhang, S. Ren, and J. Sun, "Deep residual learning for image recognition," in *Proc. CVPR*, Las Vegas, NV, USA, 2016, pp. 770–778.

[21] R. Geirhos *et al.*, "Shortcut learning in deep neural networks," *Nat. Mach. Intell.*, vol. 2, no. 11, pp. 665–673, 2020.

[22] M. F. Folstein, S. E. Folstein, and P. R. McHugh, ""mini-mental state": A practical method for grading the cognitive state of patients for the clinician," *J. Psychiatr. Res.*, vol. 12, no. 3, pp. 189–198, 1975.

[23] R. T. Rockafellar and R. J.-B. Wets, *Variational analysis*. Springer Science & Business Media, 2009, vol. 317.

[24] O. Russakovsky *et al.*, "ImageNet Large Scale Visual Recognition Challenge," *IJCV*, vol. 115, no. 3, pp. 211–252, 2015.

[25] R. Geirhos, P. Rubisch, C. Michaelis, M. Bethge, F. A. Wichmann, and W. Brendel, "Imagenet-trained cnns are biased towards texture; increasing shape bias improves accuracy and robustness," in *Proc. ICLR*, New Orleans, LA, USA, 2019.

[26] S. Sagawa, P. W. Koh, T. B. Hashimoto, and P. Liang, "Distributionally robust neural networks," in *Proc. ICLR*, Virtual, 2020.

[27] B. Y. Idrissi, M. Arjovsky, M. Pezeshki, and D. Lopez-Paz, "Simple data balancing achieves competitive worst-group-accuracy," in *Proc. CLeaR*, Eureka, CA, USA, 2022, pp. 336–351.

[28] P. Kirichenko, P. Izmailov, and A. G. Wilson, "Last layer re-training is sufficient for robustness to spurious correlations," in *Proc. ICLR*, Virtual, 2022.

[29] G. M. Hoang, U.-H. Kim, and J. G. Kim, "Vision transformers for the prediction of mild cognitive impairment to alzheimer's disease progression using mid-sagittal smri," *Front. Aging. Neurosci.*, vol. 15, p. 1102869, 2023.

[30] T. Illakiya and R. Karthik, "A dimension centric proximate attention network and swin transformer for age-based classification of mild cognitive impairment from brain mri," *IEEE Access*, vol. 11, pp. 128 018–128 031, 2023.

[31] Z. Liu, Y. Lin, Y. Cao, H. Hu, Y. Wei, Z. Zhang, S. Lin, and B. Guo, "Swin transformer: Hierarchical vision transformer using shifted windows," in *Proc. ICCV*, Virtual, 2021, pp. 10 012–10 022.

[32] M. Ashtari-Majlan, A. Seifi, and M. M. Dehshibi, "A multi-stream convolutional neural network for classification of progressive mci in alzheimer's disease using structural mri images," *IEEE J. Biomed. Health. Inf.*, vol. 26, no. 8, pp. 3918–3926, 2022.

[33] J. Bae *et al.*, "Transfer learning for predicting conversion from mild cognitive impairment to dementia of alzheimer's type based on a three-dimensional convolutional neural network," *Neurobiol. Aging.*, vol. 99, pp. 53–64, 2021.

[34] F. Gao *et al.*, "Ad-net: Age-adjust neural network for improved mci to ad conversion prediction," *NeuroImage Clin.*, vol. 27, p. 102290, 2020.

[35] M. Luo, Z. He, H. Cui, Y.-P. P. Chen, and P. Ward, "Class activation attention transfer neural networks for mci conversion prediction," *Comput. Biol. Med.*, vol. 156, p. 106700, 2023.

[36] S. K. Kim, Q. A. Duong, and J. K. Gahm, "Multimodal 3d deep learning for early diagnosis of alzheimer's disease," *IEEE Access*, vol. 12, pp. 46 278–46 289, 2024.

[37] M. Odusami, R. Maskeliūnas, R. Damaševičius, and S. Misra, "Explainable deep-learning-based diagnosis of alzheimer's disease using multimodal input fusion of pet and mri images," *J. Med. Biol. Eng.*, vol. 43, no. 3, pp. 291–302, 2023.

[38] D. Lu, K. Popuri, G. W. Ding, R. Balachandar, and M. F. Beg, "Multimodal and multiscale deep neural networks for the early diagnosis of alzheimer's disease using structural mr and fdg-pet images," *Sci. Rep.*, vol. 8, no. 1, p. 5697, 2018.

[39] S. Lee, J. Lee, M. Lee, J. Choi, K. Kang, and Y. Kim, "Integrating genetic information for early alzheimer's diagnosis through mri interpretation," in *Proc. IEEE EMBS BHI*, Pittsburgh, PA, USA, 2023, pp. 1–6.

[40] C. R. Jack Jr *et al.*, "The alzheimer's disease neuroimaging initiative (adni): Mri methods," *J. Magn. Reson. Imag.*, vol. 27, no. 4, pp. 685–691, 2008.

[41] N. J. Tustison *et al.*, "The antsx ecosystem for quantitative biological and medical imaging," *Sci. Rep.*, vol. 11, no. 1, p. 9068, 2021.

[42] N. J. Tustison *et al.*, "N4itk: Improved n3 bias correction," *IEEE Trans. Med. Imaging*, vol. 29, no. 6, pp. 1310–1320, 2010.

[43] B. B. Avants, C. L. Epstein, M. Grossman, and J. C. Gee, "Symmetric diffeomorphic image registration with cross-correlation: evaluating automated labeling of elderly and neurodegenerative brain," *Med. Image Anal.*, vol. 12, no. 1, pp. 26–41, 2008.

[44] D. Agarwal, G. Marques, I. de la Torre-Díez, M. A. Franco Martin, B. García Zapiraín, and F. Martín Rodríguez, "Transfer learning for alzheimer's disease through neuroimaging biomarkers: a systematic review," *Sensors*, vol. 21, no. 21, p. 7259, 2021.

[45] E. Perez, F. Strub, H. De Vries, V. Dumoulin, and A. Courville, "Film: Visual reasoning with a general conditioning layer," in *Proc. AAAI*, New Orleans, LA, USA, 2018.

[46] T. N. Tombaugh and N. J. McIntyre, "The mini-mental state examination: a comprehensive review," *J. Am. Geriatr. Soc.*, vol. 40, no. 9, pp. 922–935, 1992.

[47] M. Gallegos *et al.*, "45 years of the mini-mental state examination (mmse): A perspective from ibero-america," *Dement. Neuropsychol.*, vol. 16, pp. 384–387, 2022.

[48] G. L. Iverson, "Interpretation of mini-mental state examination scores in community-dwelling elderly and geriatric neuropsychiatry patients," *Int. J. Geriatr. Psychiatry*, vol. 13, no. 10, pp. 661–666, 1998.

[49] Y. Wu, Y. Zhang, X. Yuan, J. Guo, and X. Gao, "Influence of education level on mmse and moca scores of elderly inpatients," *Appl. Neuropsychol. Adult*, vol. 30, no. 4, pp. 414–418, 2023.

[50] H. Wang, H. Hsu, M. Diaz, and F. P. Calmon, "To split or not to split: The impact of disparate treatment in classification," *IEEE Transactions on Information Theory*, vol. 67, no. 10, pp. 6733–6757, 2021.

[51] M. M. Gonzales *et al.*, "Biological aging processes underlying cognitive decline and neurodegenerative disease," *J. Clin. Invest.*, vol. 132, no. 10, 2022.

[52] M. J. Cardoso *et al.*, "Monai: An open-source framework for deep learning in healthcare," *arXiv preprint arXiv:2211.02701*, 2022.

[53] A. Paszke *et al.*, "Pytorch: An imperative style, high-performance deep learning library," in *Proc. NeurIPS*, Vancouver, BC, Canada, 2019.

[54] I. Loshchilov and F. Hutter, "Decoupled weight decay regularization," in *Proc. ICLR*, New Orleans, LA, USA, 2019.

[55] A. Dosovitskiy *et al.*, "An image is worth 16x16 words: Transformers for image recognition at scale," in *Proc. ICLR*, Virtual, 2021.

[56] M. Tan and Q. Le, "Efficientnet: Rethinking model scaling for convolutional neural networks," in *Proc. ICML*, Long Beach, CA, USA, 2019, pp. 6105–6114.

[57] F. Pérez-García, R. Sparks, and S. Ourselin, "Torchio: A python library for efficient loading, preprocessing, augmentation and patch-based sampling of medical images in deep learning," *Comput. Methods Programs Biomed.*, vol. 208, p. 106236, 2021.

[58] S. Qiu *et al.*, "Development and validation of an interpretable deep learning framework for alzheimer's disease classification," *Brain*, vol. 143, no. 6, pp. 1920–1933, 2020.

[59] C. Dwork, N. Immorlica, A. T. Kalai, and M. Leiserson, "Decoupled classifiers for group-fair and efficient machine learning," in *Proc. ACM FAccT*, New York, NY, USA, 2018, pp. 119–133.

[60] C. Zhou, X. Ma, P. Michel, and G. Neubig, "Examining and combating spurious features under distribution shift," in *Proc. ICML*. Virtual: PMLR, 2021.

[61] I. Covert, S. M. Lundberg, and S.-I. Lee, "Understanding global feature contributions with additive importance measures," in *Proc. NeurIPS*, Virtual, 2020, pp. 17 212–17 223.

[62] L. McInnes, J. Healy, N. Saul, and L. Großberger, "Umap: Uniform manifold approximation and projection," *J. Open Source Softw.*, vol. 3, no. 29, p. 861, 2018.

[63] Z. S. Nasreddine *et al.*, "The montreal cognitive assessment, moca: a brief screening tool for mild cognitive impairment," *J. Am. Geriatr. Soc.*, vol. 53, no. 4, pp. 695–699, 2005.